

Article

Synthesis and Characterisation of the Europium (III) Dimolybdo-Enneatungsto-Silicate Dimer, $[\text{Eu}(\alpha\text{-SiW}_9\text{Mo}_2\text{O}_{39})_2]^{13-}$

Loïc Parent ¹, Pedro de Oliveira ², Anne-Lucie Teillout ², Anne Dolbecq ¹, Mohamed Haouas ¹, Emmanuel Cadot ¹ and Israël M. Mbomekallé ^{2,*}

¹ Institut Lavoisier de Versailles, Université de Versailles St. Quentin, UMR 8180 CNRS, Versailles, F-78035, France; E-Mails: loic.parent@uvsq.fr (L.P.); anne.dolbecq@uvsq.fr (A.D.); mohamed.haouas@uvsq.fr (M.H.); emmanuel.cadot@uvsq.fr (E.M.)

² Laboratoire de Chimie Physique, Equipe d'Electrochimie et de Photo-électrochimie, Université Paris-Sud, UMR 8000 CNRS, Orsay, F-91405, France; E-Mails: pedro.deoliveira@u-psud.fr (P.O.); anne-lucie.teillout@u-psud.fr (A.-L.T.); israel.mbomekalle@u-psud.fr (I.M.M.)

* Author to whom correspondence should be addressed; E-Mail: israel.mbomekalle@u-psud.fr; Tel.: +33-169-154-159; Fax: +33-169-156-188.

Academic Editors: Greta Ricarda Patzke and Pierre-Emmanuel Car

Received: 30 April 2015 / Accepted: 17 June 2015 / Published: 13 July 2015

Abstract: The chemistry of polyoxometalates (POMs) keeps drawing the attention of researchers, since they constitute a family of discrete molecular entities whose features may be easily modulated. Often considered soluble molecular oxide analogues, POMs possess enormous potential due to a myriad of choices concerning size, shape and chemical composition that may be tailored in order to fine-tune their physico-chemical properties. Thanks to the recent progress in single-crystal X ray diffraction, new POMs exhibiting diverse and unexpected structures have been regularly reported and described. We find it relevant to systematically analyse the different equilibria that govern the formation of POMs, in order to be able to establish reliable synthesis protocols leading to new molecules. In this context, we have been able to synthesise the Eu^{3+} -containing silico-molybdo-tungstic dimer, $[\text{Eu}(\alpha\text{-SiW}_9\text{Mo}_2\text{O}_{39})_2]^{13-}$. We describe the synthesis and characterisation of this new species by several physico-chemical methods, such as single-crystal X-ray diffraction, ^{183}W NMR and electrochemistry.

Keywords: polyoxometalates; electrochemistry; NMR; X-ray structure

1. Introduction

Polyoxometalates (POMs) are oxo-metal clusters in which the metal element M is often in its highest oxidation state ($M = W^{VI}, Mo^{VI}, V^V \dots$). Berzélius was the first to isolate a POM in 1826: the ammonium salt of the 12-molybdophosphate $[PMo_{12}O_{40}]^{3-}$ anion [1], but the first description of the structure of one of the compounds of this family, the $[PW_{12}O_{40}]^{3-}$ anion, was made more than a century later by Keggin [2]. Then, several hundreds of structures have been described, especially from the second half of the 20th century onwards. Nowadays, a myriad of new molecules, ranging from the simplest ones to unexpected and rather complex structures, are reported every year. In fact, upon modulating the experimental conditions and selecting the nature of the metal elements and their molar ratios, the different substitution and addition reactions involving POM entities with respect to metal cations offer a wide range of possibilities regarding the synthesis of new molecules which may find applications in a variety of fields such as medicine [3,4], catalysis [5,6], nanotechnologies [7,8], magnetism [9,10], *etc.* It is, then, possible and more and more common to synthesise POM species that include in their structures some elements specially selected in order to impart the features required for certain targeted applications.

Lanthanide (Ln) cations, for example, have a partially filled 4f orbital. As a consequence, they possess photoluminescence properties. In fact, they exhibit a high purity colour luminescence in the visible or in the near IR range [11], being employed in TV and computer screens, in optical fibres, *etc.* [12]. The incorporation of lanthanide cations in POMs rose a considerable interest due to the possibility of creating synergy between their electronic properties. The first POM containing a lanthanide cation as the hetero-element was the compound $[CeMo_{12}O_{42}]^{8-}$, described in 1914 [13]. Several decades later, in the beginning of the 70s, Peacock and Weakley reported the synthesis of Ln-containing POMs which formed monomers and dimers of the (POM)Ln and (POM)₂Ln types [14]. Afterwards, the family of Ln-containing POMs never ceased to grow, concomitantly becoming more and more diversified [15], on the basis of a synthesis protocol that varies little. It consists of two major steps: 1) creation of mono- or multi-lacunary POM structures which will behave as ligands; 2) co-ordination of the lanthanide cation by those ligands via oxo bridges. POM:Ln complexes are obtained, exhibiting one of the following different ratios: 1:1 [16,17], 2:1 [17–20] or 2:2 [21–23]. The most common POM structures known as Linqvist, Anderson, Keggin and Dawson may be used as lacunary species, and in some cases the co-ordination sphere of the lanthanide cation is completed by an organic ligand [24,25]. Finally, it is not unusual to come across less common structures combining fragments from different families or involving “giant” POMs [26–28]. As previously stated, the major interest of these POM:Ln compounds is to obtain a synergistic effect between the electronic properties of the POM, often considered an electron reservoir, and the lanthanide, whose 4f orbitals are partially empty. The studies of these systems are quite often focused on their luminescence properties and rarely on their electrochemical behaviour [29]. The present study concerns the synthesis, structural characterisations, electrochemical studies and electro-catalytic properties of a POM containing the Keggin fragment $[SiW_9Mo_2O_{39}]^{8-}$ and the Eu^{3+} cation, obtained as the potassium salt of the respective dimer: $K_{13}[Eu(\alpha-SiW_9Mo_2O_{39})_2] \cdot 21H_2O$. The

formation constants of this complex had already been calculated by Choppin *et al.* [30], but this is the first time that the compound has been isolated and characterised.

2. Results and Discussion

2.1. Synthesis of $K_{13}[Eu(\alpha\text{-SiW}_9\text{Mo}_2\text{O}_{39})_2] \cdot 21\text{H}_2\text{O}$

The compound $K_{13}[Eu(\alpha\text{-SiW}_9\text{Mo}_2\text{O}_{39})_2] \cdot 21\text{H}_2\text{O}$ (**1**) was prepared according to a method different from that described in the literature for its homologous species $K_{13}[Eu(\alpha\text{-SiW}_{11}\text{O}_{39})_2] \cdot 18\text{H}_2\text{O}$ [16,19]. In fact, the lacunary compound $[\alpha\text{-SiW}_9\text{Mo}_2\text{O}_{39}]^{8-}$ being less robust than its molybdenum-free homologue, the synthesis has to be carried out at room temperature and in a buffered medium (acetate buffer, pH ~4.7) in order to prevent it from decaying. Likewise, the sequence of reagent addition is reversed. The compound $[\alpha\text{-SiW}_9\text{Mo}_2\text{O}_{39}]^{8-}$ is added in small aliquots to a solution containing the Eu^{3+} ions. It may be assumed that the reaction rate between the lacunary species $[\alpha\text{-SiW}_9\text{Mo}_2\text{O}_{39}]^{8-}$ and the Eu^{3+} cation is high enough. In addition, the formation equilibrium constants determined by Choppin *et al.* [30] for POM-Eu complexes indicate that the compound $[Eu(\alpha\text{-SiW}_9\text{Mo}_2\text{O}_{39})_2]^{13-}$ is sufficiently stable in solution. This implies that the lacunary fragments $[\alpha\text{-SiW}_9\text{Mo}_2\text{O}_{39}]^{8-}$ remain free in solution for a relatively short time, which should be enough to prevent them from decomposing.

2.2. Elemental Analysis, TGA and IR Spectroscopy

The elemental analysis and the TGA results are in good agreement with the formula derived from single crystal X-ray diffraction. It consists of a potassium salt that crystallises with 21 water molecules. The main IR absorption bands observed correspond to the stretching vibrations of the X–O bonds, with X = Si or W [15,16]. The presence of Mo results in slight shifts when compared to the values reported in the study by Pope *et al.* or that by Balula and Freire cited before [15,16]. The formula of compound **1** corresponds well to that of the parent dimer $K_{13}[Eu(\alpha\text{-SiW}_{11}\text{O}_{39})_2] \cdot 18\text{H}_2\text{O}$.

2.3. Structure

The dimeric anion $[Eu(\text{SiW}_9\text{Mo}_2\text{O}_{39})_2]^{13-}$ is built of two monovacant Keggin moieties $[\alpha\text{-SiW}_9\text{Mo}_2\text{O}_{39}]^{8-}$ connected to a central Eu^{3+} cation (Figure 1A). The Mo and W centres are localised in the structure, the two MoO_6 octahedra belonging to two different trinuclear fragments and sharing a corner. The rare-earth cation is slightly off-centred of the vacant site of the $[\alpha\text{-SiW}_9\text{Mo}_2\text{O}_{39}]^{8-}$ sub-units (Figure 1B), as shown by the longer Si···Eu distance (4.52 Å) when compared to the Si···M (M = Mo, W) distances (3.48 – 3.58 Å). It may be noticed that the POM has no symmetry element and in particular is non-centrosymmetric. The local symmetry around the Eu^{3+} ion, co-ordinated by eight oxygen atoms of the Keggin fragments, is approximately square anti-prismatic (Figure 1C), as also observed, for example, in the well-known $[EuW_{10}O_{36}]^{9-}$ species [31] and also in $[Eu(\alpha\text{-SiW}_{11}\text{O}_{39})_2]^{13-}$ [29] and $[Eu(\beta_2\text{-SiW}_{11}\text{O}_{39})_2]^{13-}$ [19]. However, a pseudo C_2 axis can be identified passing through the Eu^{3+} ion (Figure 1D). Overall, the structure of $[Eu(\alpha\text{-SiW}_9\text{Mo}_2\text{O}_{39})_2]^{13-}$ is quite close to that of $[Eu(\alpha\text{-SiW}_{11}\text{O}_{39})_2]^{13-}$ [29], except for the presence of four localised Mo^{VI} centres in the former complex. However, $K_{13}[Eu(\alpha\text{-SiW}_{11}\text{O}_{39})_2] \cdot 18\text{H}_2\text{O}$ [29] and $K_{13}[Eu(\alpha\text{-SiW}_9\text{Mo}_2\text{O}_{39})_2] \cdot 21\text{H}_2\text{O}$ (**1**) are not isostructural, due to small differences in the crystal packing.

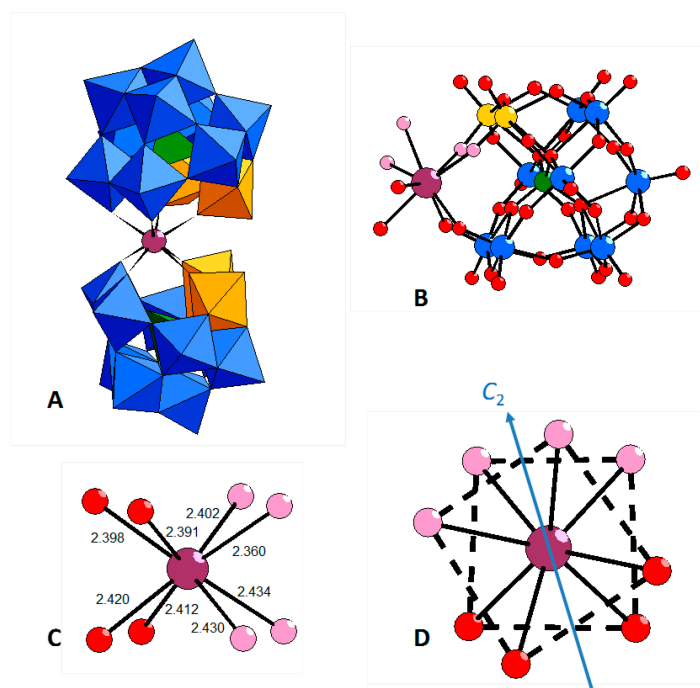


Figure 1. (A) Mixed ball-and-stick and polyhedral representation of $[\text{Eu}(\text{SiW}_9\text{Mo}_2\text{O}_{39})_2]^{13-}$; (B) ball and stick representation of the $\{(\text{SiW}_9\text{Mo}_2\text{O}_{39})\text{EuO}_4\}$ fragment; (C) environment around the Eu^{3+} ion, with the Eu-O distances (Å) indicated for each bond; (D) position of the pseudo C_2 axis passing through the Eu^{3+} ion. Blue octahedra: WO_6 ; orange octahedra: MoO_6 ; green tetrahedra: SiO_4 ; plum spheres: Eu; blue spheres: W; orange spheres: Mo; red spheres: O; pink spheres: O bound to Mo ions.

2.4. NMR Spectroscopy

Tungsten-183 (^{183}W) NMR spectroscopy allows the characterisation of the structure of $[\text{Eu}(\text{SiW}_9\text{Mo}_2\text{O}_{39})_2]^{13-}$ in solution. Figure 2 shows the ^{183}W NMR spectrum taken at 29 °C. It shows nine resonances (the monomer would exhibit five), each integrating for one W atom. This multiplicity is rather consistent with a point-group symmetry C_2 and thus a staggered conformation similar to that observed in $[\text{Ln}(\text{SiW}_{11}\text{O}_{39})_2]^{13-}$, Ln = Yb or Lu, and in opposition to the eclipsed conformation (C_{2v}) observed for Ln = La [32]. Indeed, the latter gave rise to six lines in the ^{183}W NMR spectrum, with five integrating for two W atoms and one integrating for one W atom, whereas the spectrum of the former, with either of the heavy lanthanides, exhibited eleven lines of equal intensity [32]. Thus, in the present case of the $[\text{Eu}(\text{SiW}_9\text{Mo}_2\text{O}_{39})_2]^{13-}$ species, all nine W atoms in a POM unit are not equivalent to each other and each lacunary fragment is related to the other by a two-fold rotation. Consistently, the ^{29}Si NMR spectrum shows one resonance at $\delta = -71.9$ ppm (Figure S3 in Supporting Information). Interestingly, among the nine ^{183}W lines, two of them undergo strong up-field shifts (~ -1200 ppm) that allow them to be assigned to W atoms close to the paramagnetic Eu centre. The other two metal centres bridged to Eu through metal-oxo junctions are then the two Mo atoms, in agreement with X-ray diffraction analysis. Also, six of the remaining ^{183}W lines are relatively broad (line width $\sim 5\text{--}8$ Hz), presumably as a consequence of residual paramagnetic interaction. Finally, the last line at $\delta = -127.4$ ppm is

very narrow (line width <1 Hz) and even exhibits ${}^2J_{\text{W-O-W}}$ coupling satellites (${}^2J = 16$ Hz). It should, thus, be attributed to the W atom positioned at the longest distance from the Eu centre.

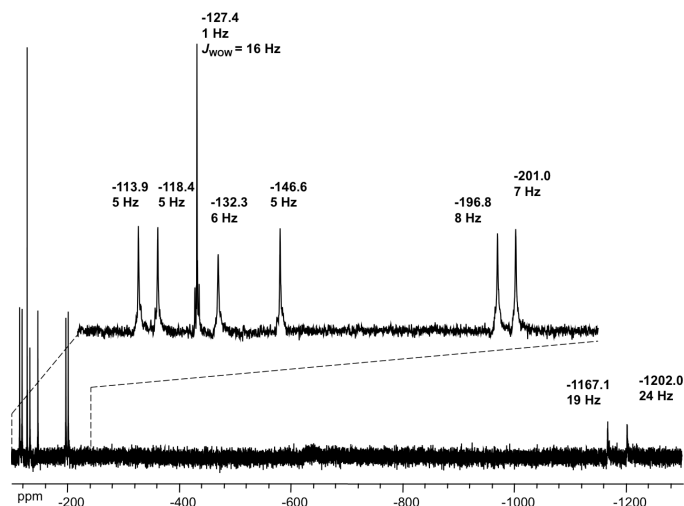


Figure 2. ${}^{183}\text{W}$ NMR spectrum of the lithium salt of $[\text{Eu}(\text{SiW}_9\text{Mo}_2\text{O}_{39})_2]^{13-}$ in $\text{D}_2\text{O}/\text{H}_2\text{O}$ solution.

2.5. Electrochemistry

Compound **1** is stable at pH 3 in lithium sulphate solution. For lower pH values (see SI), it slowly decomposes to give rise to the saturated species $[\text{SiW}_9\text{Mo}_3\text{O}_{40}]^{4-}$. Figure 3 shows the CVs of **1** and of $[\text{SiW}_9\text{Mo}_2\text{O}_{39}]^{8-}$ recorded in the same experimental conditions and restricted to the redox processes attributed to the Mo^{VI} centres of the two compounds. The CV of **1** shows a quasi-reversible wave with $E_{\text{pc}} = -0.170$ V vs. SCE and $\Delta E = 0.070$ V ($\Delta E = E_{\text{pa}} - E_{\text{pc}}$). The CV of $[\text{SiW}_9\text{Mo}_2\text{O}_{39}]^{8-}$ reveals a slower process taking place at far more negative potentials, -0.396 V vs. SCE. It is a rather irreversible process when compared to that of compound **1**.

We were taken aback by the shape of the re-oxidation wave of **1**, which suggests that there is a desorption step subsequent to the formation of a film on the surface of the working electrode. In order to sort this out, we studied the dependence of the oxidation peak current intensity, I_{pa} , as a function of the scan rate, ν (Figure S4-A). The plot of I_{pa} as a function of ν does not give a straight line, as should be the case for a simple adsorbed species mechanism (Figure S4-B). Likewise, the plot of I_{pa} as a function of the square root of the scan rate, $\nu^{1/2}$, is not a straight line either (Figure S4-C), as expected from the shape of the re-oxidation wave. It is highly likely that the overall process is simultaneously controlled by diffusion and adsorption phenomena. This sort of mechanism has been previously described by Amatore *et al.* for certain electro-catalytic processes [33].

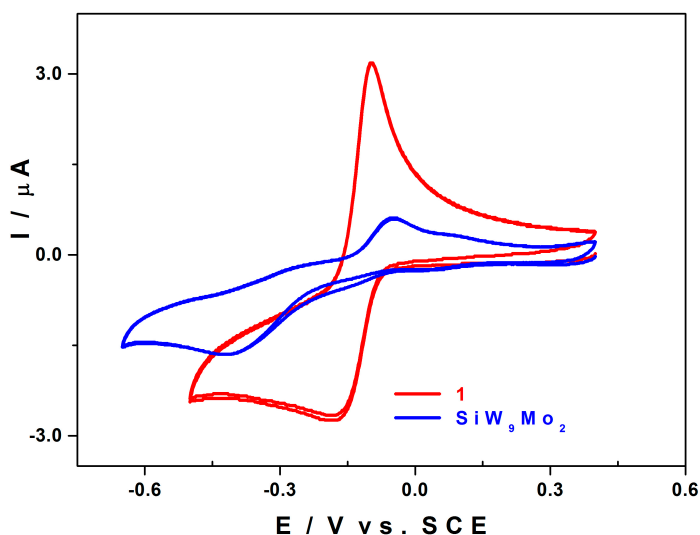


Figure 3. CVs of **1** (red) and of $[\text{SiW}_9\text{Mo}_2\text{O}_{39}]^{8-}$ (blue) in 0.5 M $\text{Li}_2\text{SO}_4 + \text{H}_2\text{SO}_4/\text{pH } 3$. Scan rate: $10 \text{ mV}\cdot\text{s}^{-1}$. POM concentration: $2.5 \times 10^{-4} \text{ M}$; working electrode: EPG; counter electrode: Pt; reference electrode: SCE.

A controlled potential coulometry experiment carried out at -0.40 V vs. SCE yielded a consumption of 4 moles of electrons per mole of **1**, meaning that the Mo^{VI} centres in compound **1** are all reduced to Mo^{V} by the uptake of an electron each, the solution becoming violet (Figure S5-A). Upon resetting the potential to $+0.30 \text{ V vs. SCE}$, a re-oxidation step ensues in which over 95% of the previously consumed charge is recovered, and the solution reverts to its initial colourless aspect. The CVs recorded between these different steps show that compound **1** does not decompose when undergoing its reduction followed by its re-oxidation (Figure S5-B). Beyond this first redox wave, there is a large irreversible process having a reduction peak potential at -0.860 V vs. SCE (Figure S6).

We found it interesting to compare the response of the species **1** with that of its parent compound, the Keggin-type silico-tungstic derivative possessing three Mo^{VI} centres, $[\text{SiW}_9\text{Mo}_3\text{O}_{40}]^{4-}$, as far as their redox and electro-catalytic properties are concerned.

2.5.1. Compared Redox Behaviour of **1** and of $[\text{SiW}_9\text{Mo}_3\text{O}_{40}]^{4-}$ at pH 3.0

Figure 4 shows the CVs of **1** and of $[\text{SiW}_9\text{Mo}_3\text{O}_{40}]^{4-}$ in 0.5 M $\text{Li}_2\text{SO}_4 + \text{H}_2\text{SO}_4/\text{pH } 3$. Even if the three Mo^{VI} centres of the compound $[\text{SiW}_9\text{Mo}_3\text{O}_{40}]^{4-}$ are equivalent, their overall reduction does not take place in a single step, as is the case for compound **1**. In fact, the CV of $[\text{SiW}_9\text{Mo}_3\text{O}_{40}]^{4-}$ reveals three successive single-electron waves corresponding to the one-electron reduction of each of the Mo^{VI} centres. We recall that we observed a single four-electron redox wave for compound **1** in the same experimental conditions. The symmetry of compound **1** implies that the four Mo^{VI} centres are divided into two equivalent groups, each comprising two Mo^{VI} centres whose molecular orbitals have the same energy when the molecule is in its oxidised state. The uptake of four electrons, despite being fast, corresponds to a multi-step process, as is the case for all multi-electron reductions. We would expect to observe a decrease of the level of degeneracy after the uptake of the first electron, resulting in the splitting of the initial single wave into several waves: a sequence of either two two-electron steps or four single-electron steps. The latter phenomenon is observed upon the reduction of the three Mo^{VI} centres

of the compound $[\text{SiW}_9\text{Mo}_3\text{O}_{40}]^{4-}$, which are equivalent when the molecule is in its highest oxidation state, but whose degree of degeneracy decreases when the first electron is added. There are three successive single-electron reduction waves in the CV of $[\text{SiW}_9\text{Mo}_3\text{O}_{40}]^{4-}$, whereas that of compound **1** reveals a single four-electron wave in the same experimental conditions. The degree of degeneracy is not affected in the latter, the four Mo centres remaining equivalent throughout the addition of the four electrons.

This behaviour should have a beneficial influence on the electro-catalytic properties of **1**. Indeed, the most promising compounds for electro-catalysis are those capable of exchanging a large number of electrons in one go.

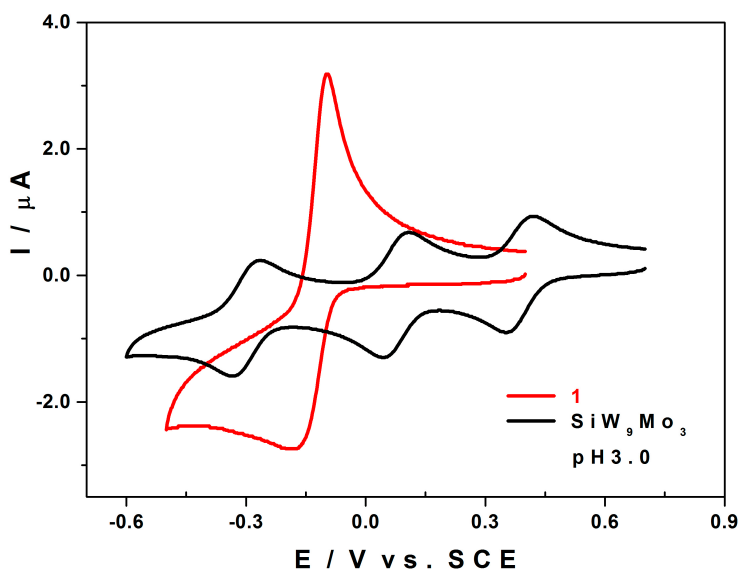


Figure 4. CVs of **1** (red) and of $[\text{SiW}_9\text{Mo}_3\text{O}_{40}]^{4-}$ (black) in 0.5 M $\text{Li}_2\text{SO}_4 + \text{H}_2\text{SO}_4/\text{pH } 3$. Scan rate: $10 \text{ mV}\cdot\text{s}^{-1}$. POM concentration: $2.5 \times 10^{-4} \text{ M}$. Working electrode: EPG; counter electrode: Pt; reference electrode: SCE.

2.5.2. Electro-Catalytic Activity of **1** towards O_2 and H_2O_2 Reduction

We were also interested in the electro-catalytic efficiency of compound **1** with respect to the reduction of both dioxygen (O_2) and hydrogen peroxide (H_2O_2). In fact, it is important to check these two processes and to compare their respective onset potentials, that is, the potential values at which the electro-catalytic reactions start. In the case of the species **1**, the onset potential for the reduction of H_2O_2 is less negative than that for O_2 . This means that the electro-reduction of H_2O_2 on an EPG electrode is easier than that of O_2 in the presence of compound **1**. When we concentrate on the electro-reduction of O_2 , the overall process will be pursued beyond the formation of H_2O_2 up to H_2O as the final product.

Figure 5A confirms that the reduction of H_2O_2 is easier than that of O_2 . Also, the efficiency of H_2O_2 reduction increases upon successive cycling (Figure 5B). The working electrode surface activation is probably due to the formation of a deposit that does not totally re-dissolve in the presence of H_2O_2 . In the case of the electro-reduction of O_2 , the activation phenomenon is not observed, the successive CVs being superposable (Figure S7). This suggests that the process of electro-catalytic reduction of O_2 by compound **1** either does not include a H_2O_2 formation step or H_2O_2 is a transient species whose lifespan

is so short that no activation film forms on the electrode surface, meaning that the response shown in Figure 5B is not observed.

This activation phenomenon is not observed with the species $[\text{SiW}_9\text{Mo}_3\text{O}_{40}]^{4-}$ and its onset potential for the reduction of H_2O_2 is more negative than that for the reduction of O_2 (Figure 8S-A). It is also important to point out that for the electro-catalytic reduction processes of both O_2 and H_2O_2 , compound **1** is always more efficient than the parent species $[\text{SiW}_9\text{Mo}_3\text{O}_{40}]^{4-}$ (Figure 8S-B).

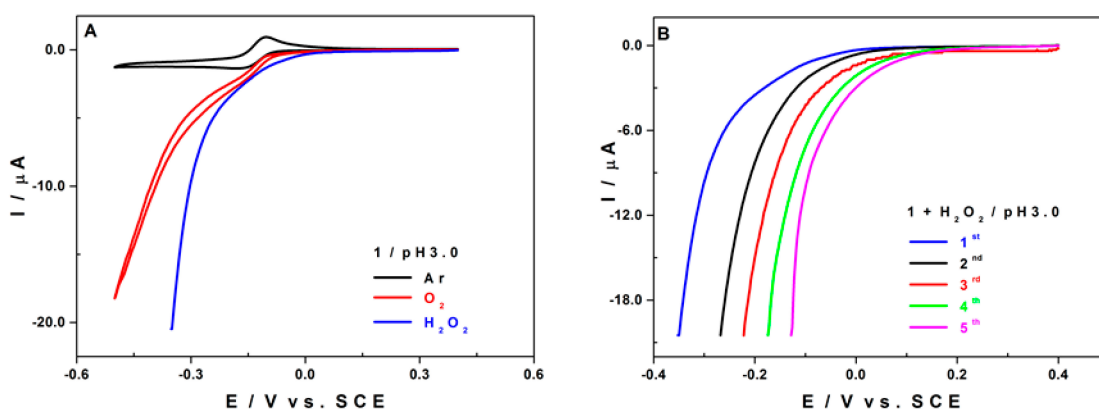


Figure 5. (A) CVs of **1** alone in an argon saturated solution (black), in a O_2 saturated solution (red), and in the presence of 0.25 M H_2O_2 (blue) in 0.5 M $\text{Li}_2\text{SO}_4 + \text{H}_2\text{SO}_4/\text{pH } 3$. (B) Successive CVs of **1** in the presence of 0.25 M H_2O_2 in 0.5 M $\text{Li}_2\text{SO}_4 + \text{H}_2\text{SO}_4/\text{pH } 3$. Scan rate: $2 \text{ mV}\cdot\text{s}^{-1}$. POM concentration: $2.5 \times 10^{-4} \text{ M}$. Working electrode: EPG; counter electrode: Pt; reference electrode: SCE.

3. Experimental Section

3.1. Synthesis of $\text{K}_{13}[\text{Eu}(\alpha\text{-SiW}_9\text{Mo}_2\text{O}_{39})_2] \cdot 21\text{H}_2\text{O}$

0.18 g of $\text{EuCl}_3 \cdot 6\text{H}_2\text{O}$ (0.5 mmol) are dissolved in 30 mL of 0.5M $\text{NaCH}_3\text{COO} + 0.5\text{M } \text{CH}_3\text{COOH}/\text{pH } 4.7$, and then 3.0 g of $\text{K}_8[\alpha\text{-SiW}_9\text{Mo}_2\text{O}_{39}] \cdot n\text{H}_2\text{O}$ (1 mmol) are added in small aliquots. This procedure is adapted from the method described by Cadot *et al.* [34]. The mixture is stirred at room temperature until the dissolution is complete, and then filtered. After a few days, needle-like white crystals form in the colourless filtrate, which are recovered by filtration and dried in the open air. A mass of 1.24 g of the white crystals of the compound $\text{K}_{13}[\text{Eu}(\alpha\text{-SiW}_9\text{Mo}_2\text{O}_{39})_2] \cdot 21\text{H}_2\text{O}$ was obtained, corresponding to a yield of 41%. IR (cm^{-1}): 1003(w), 940 (m), 884 (s), 813 (m), 755 (m), 713 (m), 528 (w).

3.2. TGA, and IR Spectroscopy

Hydration water contents were determined by thermogravimetric analysis performed in a nitrogen atmosphere between 25 and 600 $^\circ\text{C}$, with a heating speed of $5 \text{ }^\circ\text{C}\cdot\text{min}^{-1}$, using a Metler Toledo TGA/DSC1.. Infrared spectra were recorded on a Nicolet 6700 FT spectrometer driven by a PC with the OMNIC E.S.P. 8.2 software.

3.3. X-ray Crystallography

Data collection was carried out using a Siemens SMART three-circle diffractometer equipped with a CCD bi-dimensional detector using the monochromatised wavelength $\lambda(\text{Mo K}\alpha) = 0.71073 \text{ \AA}$. Absorption correction was based on multiple and symmetry-equivalent reflections in the data set using the SADABS program [35] based on the method of Blessing [36]. The structure was solved by direct methods and refined by full-matrix least-squares using the SHELX-TL package [37]. There is a discrepancy between the formulae determined by elemental analysis and that deduced from the crystallographic atom list because of the difficulty in locating all the disordered water molecules and counter-ions. These disordered water molecules and counter-ions, when located, were refined isotropically and with partial occupancy factors. Crystallographic data are given in Table 1. Further details of the crystal structure investigation may be obtained from the Fachinformationszentrum Karlsruhe, D-76344 Eggenstein-Leopoldshafen (Germany), on quoting the depository number CSD-429499.

Table 1. Crystallographic data.

Parameters	1
Formula	$\text{EuK}_{13}\text{Mo}_4\text{O}_9\text{Si}_2\text{W}_{18}$
Formula weight, g	5913.50
Crystal system	triclinic
Space group	<i>P</i> -1
<i>a</i> /Å	12.2447(10)
<i>b</i> /Å	12.7803(10)
<i>c</i> /Å	33.762(3)
α /°	83.799(2)
β /°	85.106(2)
γ /°	66.214(2)
<i>V</i> /Å ³	4801.4(6)
<i>Z</i>	2
<i>D</i> _{calc} /g cm ⁻³	4.090
μ /mm ⁻¹	23.307
Data/parameters	37169/26808
<i>R</i> _{int}	0.0560
GOF	0.946
<i>R</i> ₁ (<i>I</i> > 2σ(<i>I</i>))	0.0720
<i>wR</i> ₂	0.1786

3.4. NMR Spectroscopy

The NMR spectra were obtained on a Bruker AVANCE-400 spectrometer using a 10 mm broad-band probe. The ¹⁸³W spectrum at 16.7 MHz was recorded with a spectral width of 100 kHz, an acquisition time of 0.7 s, a pulse delay of 0.2 s, a pulse width of 50 μs (90° tip angle) and a number of scans of 131072. The ²⁹Si spectrum at 79.5 MHz was recorded with a spectral width of 4 kHz, an acquisition time of 0.5 s, a pulse delay of 0.1 s, a pulse width of 14 μs (90° tip angle) and a number of scans of 16384. For all spectra, the temperature was controlled and fixed at 29 °C. The ¹⁸³W spectrum was referenced to

2.0 mol.dm⁻³ Na₂WO₄ and the ²⁹Si spectrum to SiMe₄. For the ²⁹Si and the ¹⁸³W chemical shifts, the convention used is that the more negative chemical shifts denote up-field resonances.

3.5. Electrochemistry

Pure water was obtained with a Milli-Q Intregal 5 purification set. All reagents were of high-purity grade and were used as purchased without further purification: H₂SO₄ (Sigma Aldrich) and Li₂SO₄ H₂O (Acros Organics). The composition of the electrolyte was 0.5 M Li₂SO₄ + H₂SO₄/pH 3.0.

The stability of polyanions **1**, [α-SiW₉Mo₂O₃₉]⁸⁻ and [SiW₉Mo₃O₄₀]⁴⁻ in solution in this medium was long enough to allow their characterisation by cyclic voltammetry and control potential coulometry. The UV-visible spectra were recorded on a Perkin-Elmer 750 spectrophotometer with 10⁻⁴ M solutions of the polyanion. Matched 2.00 mm optical path quartz cuvettes were used.

Electrochemical data were obtained using an EG & G 273 A potentiostat driven by a PC with the M270 software. A one-compartment cell with a standard three-electrode configuration was used for cyclic voltammetry experiments. The reference electrode was a saturated calomel electrode (SCE) and the counter electrode a platinum gauze of large surface area; both electrodes were separated from the bulk electrolyte solution via fritted compartments filled with the same electrolyte. The working electrodes were a 3 mm OD pyrolytic carbon disc or a ca. 10 × 10 × 2 mm³ glassy carbon stick (Le Carbone-Lorraine, France). The pre-treatment of the first electrode before each experiment is adapted from a method described elsewhere [38]. The stick is polished twice with SiC paper, grit 500 (Struers). After each polishing step, which lasts for about 5 min, the stick is rinsed and sonicated twice in Millipore water for a total of 10 minutes. Prior to each experiment, solutions were thoroughly de-aerated for at least 30 minutes with pure Ar. A positive pressure of this gas was maintained during subsequent work. All cyclic voltammograms were recorded at a scan rate of 10 mV.s⁻¹ and potentials are quoted against the saturated calomel electrode (SCE) unless otherwise stated. The polyanion concentration was × 10⁻⁴ M. All experiments were performed at room temperature, which is controlled and fixed for the laboratory at 20°C. Results were very reproducible from one experiment to the other and slight variations observed over successive runs are rather attributed to the uncertainty associated with the detection limit of our equipment (potentiostat, hardware and software) and not to the working electrode pre-treatment nor to possible fluctuations in temperature.

4. Conclusions

In an acetate buffer medium, the mono-lacunary polyanion [α-SiW₉Mo₂O₃₉]⁸⁻ reacts with the Eu³⁺ cation, giving rise to the dimer species [Eu(α-SiW₉Mo₂O₃₉)₂]¹³⁻. This new compound was characterised by several physico-chemical methods, such as TGA and IR spectroscopy, which allowed us to infer its chemical formula, K₁₃[Eu(α-SiW₉Mo₂O₃₉)₂].21H₂O. Single crystal X ray diffraction, ¹⁸³W and ²⁹Si NMR results are coherent with the fact that the compound is made of two [α-SiW₉Mo₂O₃₉]⁸⁻ fragments which co-ordinate the Eu³⁺ cation via 8 atoms.

The structure of compound **1** shows that there are two sorts of equivalent Mo centres, but the cyclic voltammetry revealed that they are all simultaneously reduced, contrary to the results observed with the parent compound [α-SiW₉Mo₃O₄₀]⁴⁻, for which there are three reduction steps corresponding to the three

Mo centres. Compound **1** exhibits a good catalytic efficiency towards the reduction of O₂ and H₂O₂.

Supplementary Materials

Additional experimental data: UV-visible spectra of **1**, SiW₉Mo₂ and EuCl₃·6H₂O (Figure S1), TGA curve of **1** (Figure S2), ²⁹Si NMR spectrum of **1** (Figure S3), additional electrochemical data (Figures S4-S8).

Acknowledgments

This work was supported by the Centre National de la Recherche Scientifique (UMR 8000, UMR 8180), the University of Paris-Sud and the University of Versailles.

Author Contribution

The preparation of the manuscript was made by all authors. L.P.: Syntheses, electrochemical and Electrocatalytic studies. P.d.O.: Careful follow-up and improvement of the manuscript. A.-L.T.: Electrochemical and electrocatalytic studies. A.D.: Single crystal X-ray diffraction and wrote that part. M.H.: NMR studies and wrote that part. E.C.: Careful follow-up and improvement of the manuscript. I.M.M.: General idea and plan for the publication.

Conflicts of Interest

The authors declare no conflict of interest.

References

1. Berzelius, J.J. Beitrag zur näheren Kenntniss des Molybdäns. *Ann. Phys.* **1826**, *82*, 369–392 (In German).
2. Keggin, J.F. Structure of the Molecule of 12-Phosphotungstic. *Nature* **1933**, *131*, 908–909.
3. Rhule, J.T.; Hill, C.L.; Judd, D.A.; Schinazi, R.F. Polyoxometalates in Medicine. *Chem. Rev.* **1998**, *98*, 327–358.
4. Prudent, R.; Moucadel, V.; Laudet, B.; Barette, C.; Lafanechère, L.; Hasenknopf, B.; Li, J.; Bareyt, S.; Lacôte, E.; Thorimbert, S.; Malacria, M.; Gouzerh, P.; Cochet, C. Identification of polyoxometalates as nanomolar noncompetitive inhibitors of protein kinase CK2. *Chem. Biol.* **2008**, *15*, 683–692.
5. Lv, H.; Geletii, Y.V.; Zhao, C.; Vickers, J.W.; Zhu, G.; Luo, Z.; Song, J.; Lian, T.; Musaev, D.G.; Hill, C.L. Polyoxometalate water oxidation catalysts and the production of green fuel. *Chem. Soc. Rev.* **2012**, *41*, 7572–7589.
6. Mizuno, N.; Kamata, K. Catalytic oxidation of hydrocarbons with hydrogen peroxide by vanadium-based polyoxometalates. *Coord. Chem. Rev.* **2011**, *255*, 2358–2370.

7. Mitchell, S.G.; de la Fuente, J.M. The synergistic behavior of polyoxometalates and metal nanoparticles: from synthetic approaches to functional nanohybrid materials. *J. Mater. Chem.* **2012**, *22*, 18091–18100.
8. Mondloch, J.E.; Bayram, E.; Finke, R.G. A review of the kinetics and mechanisms of formation of supported-nanoparticle heterogeneous catalysts. *J. Mol. Catal. A* **2012**, *355*, 1–38.
9. Oms, O.; Dolbecq, A.; Mialane, P. Diversity in structures and properties of 3d-incorporating polyoxotungstates. *Chem. Soc. Rev.* **2012**, *41*, 7497–7536.
10. Zheng, S.-T.; Yang, G.-Y. Recent advances in paramagnetic-TM-substituted polyoxometalates (TM = Mn, Fe, Co, Ni, Cu). *Chem. Soc. Rev.* **2012**, *41*, 7623–7646.
11. Bünzli, J.-C.G.; Piguet, C. Taking advantage of luminescent lanthanide ions. *Chem. Soc. Rev.* **2005**, *34*, 1048–1077.
12. Binnemans, K. Lanthanide-based luminescent hybrid materials. *Chem. Rev.* **2009**, *109*, 4283–4374.
13. Barbieri, G.A. The position of cerium in the periodic system and the complex molybdates of tetravalent cerium, Atti della Accademia Nazionale dei Lincei, Classe di Scienze Fisiche. *Mat. Nat. Rend.* **1914**, *23*, 805–812 (In Italian).
14. Peacock, R.D.; Weakley, T.J.R. Heteropolytungstate complexes of the lanthanide elements. Part I. Preparation and reactions. *J. Chem. Soc. A* **1971**, 1836–1839.
15. Granadeiro, C.M.; de Castro, B.; Balula, S.S.; Cunha-Silva, L. Lanthanopolyoxometalates: From the structure of polyanions to the design of functional materials. *Polyhedron* **2013**, *52*, 10–24.
16. Sadakane, M.; Dickman, M.; Pope, M. Controlled Assembly of Polyoxometalate Chains from Lacunary Building Blocks and Lanthanide-Cation Linkers. *Angew. Chem. Int. Ed.* **2000**, *39*, 2914–2916.
17. Luo, Q.; Howell, R.C.; Bartis, J.; Dankova, M.; Horrocks, W.D.; Rheingold, A.L.; Francesconi, L.C. Lanthanide Complexes of $[\alpha\text{-}2\text{-P}_2\text{W}_{17}\text{O}_{61}]^{10-}$: Solid State and Solution Studies. *Inorg. Chem.* **2002**, *41*, 6112–6117.
18. Gaunt, A.J.; May, I.; Sarsfield, M.J.; Collison, D.; Helliwell, M.; Denniss, I.S. A rare structural characterisation of the phosphomolybdate lacunary anion, $[\text{PMo}_{11}\text{O}_{39}]_7^-$. Crystal structures of the Ln(III) complexes, $(\text{NH}_4)_{11}[\text{Ln}(\text{PMo}_{11}\text{O}_{39})_2] \cdot 16\text{H}_2\text{O}$ (Ln = Ce^{III}, Sm^{III}, Dy^{III} or Lu^{III}) Electronic supplementary information (ESI) available: IR. *Dalton Trans.* **2003**, 2767–2771.
19. Bassil, B.S.; Dickman, M.H.; von der Kammer, B.; Kortz, U. The monolanthanide-containing silicotungstates $[\text{Ln}(\beta_2\text{-SiW}_{11}\text{O}_{39})_2]^{13-}$ (Ln = La, Ce, Sm, Eu, Gd, Tb, Yb, Lu): a synthetic and structural investigation. *Inorg. Chem.* **2007**, *46*, 2452–2458.
20. Ostuni, A.; Bachman, R.E.; Pope, M.T. Multiple Diastereomers of $[\text{M}^{n+}(\alpha_m\text{-P}_2\text{W}_{17}\text{O}_{61})_2]^{(20-n)-}$ (M = U^{IV}, Th^{IV}, Ce^{III}; m = 1, 2). *Syn- and Anti-Conformations of the Polytungstate Ligands in $\alpha_1\alpha_1$, $\alpha_1\alpha_2$ and $\alpha_2\alpha_2$ Complexes.* *J. Clust. Sci.* **2003**, *14*, 431–446.
21. Niu, J.; Wang, K.; Chen, H.; Zhao, J.; Ma, P.; Wang, J.; Li, M.; Bai, Y.; Dang, D. Assembly Chemistry between Lanthanide Cations and Monovacant Keggin Polyoxotungstates: Two Types of Lanthanide Substituted Phosphotungstates $[\{(\alpha\text{-PW}_{11}\text{O}_{39}\text{H})\text{Ln}(\text{H}_2\text{O})_3\}_2]^{6-}$ and $[\{(\alpha\text{-PW}_{11}\text{O}_{39})\text{Ln}(\text{H}_2\text{O})(\eta^2, \mu\text{-}1, 1)\text{-CH}_3\text{COO}\}_2]^{10-}$. *Cryst. Growth Des.* **2009**, *9*, 4362–4372.

22. Sadakane, M.; Ostuni, A.; Pope, M.T. Formation of 1:1 and 2:2 complexes of Ce(III) with the heteropolytungstate anion α_2 -[P₂W₁₇O₆₁]¹⁰⁻, and their interaction with proline. The structure of [Ce₂(P₂W₁₇O₆₁)₂(H₂O)₈]¹⁴⁻. *Dalt. Trans.* **2002**, 63–67.
23. Zhang, C.; Bensaid, L.; McGregor, D.; Fang, X.; Howell, R.C.; Burton-Pye, B.; Luo, Q.; Todaro, L.; Francesconi, L.C. Influence of the Lanthanide Ion and Solution Conditions on Formation of Lanthanide Wells–Dawson Polyoxotungstates. *J. Clust. Sci.* **2006**, *17*, 389–425.
24. Kortz, U. Rare-Earth Substituted Polyoxoanions: [La(CH₃COO)(H₂O)₂(2-P₂W₁₇O₆₁)]₂¹⁶⁻ and [Nd(H₂O)₃(α_2 -P₂W₁₇O₆₁)]₂¹⁴⁻. *J. Clust. Sci.* **2003**, *14*, 205–214.
25. Mialane, P.; Dolbecq, A.; Marrot, J.; Sécheresse, F. Oligomerization of Yb(III)-substituted Dawson polyoxotungstates by oxalato ligands. *Inorg. Chem. Commun.* **2005**, *8*, 740–742.
26. Dickman, M.H.; Gama, G.J.; Kim, K.; Pope, M.T. The structures of europium(III)- and uranium(IV) derivatives of [P₅W₃₀O₁₁₀]¹⁵⁻: Evidence for “cryptohydration”. *J. Clust. Sci.* **1996**, *7*, 567–583.
27. Naruke, H.; Yamase, T. Crystal structure of K_{18.5}H_{1.5}[Ce₃(CO₃)(SbW₉O₃₃)(W₅O₁₈)₃] 14H₂O. *J. Alloys Compd.* **1998**, *268*, 100–106.
28. Müller, A.; Beugholt, C.; Bögge, H.; Schmidtman, M. Influencing the Size of Giant Rings by Manipulating Their Curvatures: Na₆[Mo₁₂₀O₃₆₆(H₂O)₄₈H₁₂{Pr(H₂O)₅}]₆ (~200H₂O) with Open Shell Metal Centers at the Cluster Surface. *Inorg. Chem.* **2000**, *39*, 3112–3113.
29. Julião, D.; Fernandes, D.M.; Cunha-Silva, L.; Ananias, D.; Balula, S.S.; Freire, C. Sandwich lanthano-silicotungstates: Structure, electrochemistry and photoluminescence properties. *Polyhedron* **2013**, *52*, 308–314.
30. VanPelt, C.E.; Crooks, W.J.; Choppin, G.R. Stability constant determination and characterization of the complexation of trivalent lanthanides with polyoxometalates. *Inorg. Chim. Acta* **2003**, *346*, 215–222.
31. Yamase, T.; Ozeki, T.; Ueda, K. Structure of NaSr₄[EuW₁₀O₃₆] 34.5H₂O. *Acta Cryst.* **1993**, *C49*, 1572–1574.
32. Bartis, J.; Sukal, S.; Dankova, M.; Kraft, E.; Kronzon, R.; Blumenstein, M.; Francesconi, L.C. Lanthanide complexes of polyoxometalates: characterization by tungsten-183 and phosphorus-31 nuclear magnetic resonance spectroscopy. *Dalton Trans.* **1997**, 1937–1944.
33. Klymenko, O.V.; Svir, I.; Amatore, C. Molecular electrochemistry and electrocatalysis: a dynamic view. *Mol. Phys.* **2014**, *112*, 1273–1283.
34. Cadot, E.; Thouvenot, R.; Teze, A.; Herve, G. Syntheses and multinuclear NMR characterizations of α -[SiMo₂W₉O₃₉]⁸⁻ and α -[SiMo_{3-x}V_xW₉O₄₀]^{(4+x)-} (x = 1, 2) heteropolyoxometalates. *Inorg. Chem.* **1992**, *31*, 4128–4133.
35. Sheldrick, G.M. *SADABS*, program for scaling and correction of area detector data; University of Göttingen: Germany 1997.
36. Blessing, R.H. An empirical correction for absorption anisotropy. *Acta Cryst.* **1995**, *C51*, 33–38.
37. Sheldrick, G.M. *SHELX-TL*, version 5.03; Software Package for the Crystal Structure Determination; Siemens Analytical X-ray Instrument Division: Madison, WI, USA, 1994.

38. Vilà, N.; Aparicio, P.A.; Sécheresse, F.; Poblet, J.M.; López, X.; Mbomekallé, I.M. Electrochemical behavior of α_1/α_2 -[Fe(H₂O)P₂W₁₇O₆₁]⁷⁻ isomers in solution: experimental and DFT studies. *Inorg. Chem.* **2012**, *51*, 6129–6138.

© 2015 by the authors; licensee MDPI, Basel, Switzerland. This article is an open access article distributed under the terms and conditions of the Creative Commons Attribution license (<http://creativecommons.org/licenses/by/4.0/>).